Integrating Network Pharmacology and MALDI-MSI Spatial Metabolomics Revealing Ellagic Acid as the Key AntiPharyngitis Agent in Fructus Chebulae and its Key Metabolic Pathways in Pharyngeal Tissues

Yifei Kong[a], Chao Wang[a], Ya Zhang[a], Xingping Luo[b], Fangdi Hu[a*], Juan Chen[a], Xinyue Chen[a*]

[a]School of Pharmacy, Lanzhou University, Lanzhou 730000, P.R. China

[b]Northwest Minzu University, Lanzhou University, Lanzhou 730000, P.R. China

(The video file of "Dynamic display of the throat of mice" was also uploaded as another supplementary material, but it cannot be converted to PDF, please view this file on line)

Corresponding author: Fangdi Hu, No. 222, Tianshui Road, Lanzhou City, Gansu Province, China
E-mail: hufd @lzu.edu.cn, Tel: +86-13819780068
Corresponding author: Juan Chen, No. 222, Tianshui Road, Lanzhou City, Gansu Province, China
E-mail: chenjuan@lzu.edu.cn, Tel: +86-13008728321
Corresponding author: Xinyue Chen, No. 222, Tianshui Road, Lanzhou City, Gansu Province, China
E-mail: chenxinyue888@126.com, Tel: +86-15293109642

2 Experimental procedures

2.1 Laboratory animals and reagents

Healthy 21-day-old male KM mice were purchased from the Medical Experimental Center of Lanzhou University (weight 28.0 ± 0.5 g, n=2). Animals were kept in air-conditioned rooms at 20 ±2 ℃and 53 ± 5 % relative humidity, providing a 12 h dark/12 h light cycle and eating freely. After 5 days of adaptive feeding, the mice were fasted for one day. All procedures and experimental protocols were approved by the Ethical Committee of Animal Care and Use, Lanzhou University (Certificate No.SCXK (gan) 2018-0002) and were carried out in accordance with international standards and the ethical guidelines for animal welfare.

Standards of ellagic acid were purchased from Shanghai Yuanye Biotechnology Co., Ltd (Shanghai, China), Purity > 98%; Lan Qin oral liquid were purchased from Yangzijiang Pharmaceutical Group Co.; 25% ammonia (Tianjin ,China); Paraformaldehyde (Tianjin ,China); Gelatin was provided by Tianjin Kemiou Chemical Reagent Co., Ltd (Tianjin, China); Dewaxing liquid (Wuxi, China); Anhydrous ethanol (Tianjin China), Sealed goat serum (Beijing China), Sodium citrate buffer (Beijing China); PBS Phosphate Buffer (Shangwei Biologicals Co.) Fluorescent Secondary Antibody (488) (Immunoway Antibodies Co.); DAPI (Beijing Solepol Biotechnology Co.) Antifluorescence Attenuation Sealer (Beijing Solebo Biotechnology Co.) Hematoxylin (Isejyu Biologicals); Yihong (Tianjin Tianxin Fine Chemical Development Centre); Neutral Gum (Beijing Solebao Biotechnology Co.) Scutellaria Blue Oral Liquid(Yangzijiang Pharmaceutical Group Co.);DMSO(Tianjin Damao Chemical Reagent Factory); Mice Tumour Necrosis Factor-α (TNF-α) ELISA Research Kit was purchased from (Jiangsu Enzyme Immunity Industry Co.) Mice SOD reagent kit (WST-1 method) and Mice Malondialdehyde (MDA) Assay Kit (TBA method) was purchased from Nanjing Jianjian Bioengineering Research Institute. BCA protein concentration determination kit was purchased from Beijing Solebaum Biotechnology Co. Conductive Indium Tin Oxide (ITO) Slides Square was purchased from South China Technology Co. (Resistance ≤ 5 Ω); α-Cyano-4-hydroxycinnamic acid (CHCA) was purchased from Shanghai Titan Technology Co.; Trifluoroacetic acid was purchased from Sigma Aldrich Co.; Carrying broken tablets were purchased from Jiangsu Shitai Experimental Equipment Co;

2.3 Instruments, databases and analysis software

Slicer was purchased from Jinhua Yidi Medical Equipment Co., Ltd; Tissue Spreader, Biological Tissue Freezing and Embedding Machine were purchased from Jinhua Yidi Medical Equipment Co., Ltd; Microscope Scanning System was purchased from Ningbo Jiangfeng Biological Information Technology Co. HITACHI was

purchased from Japan; Freezing-microtome was obtained from Fisher Scientific (Loughborough, UK). Automatic matrix spraying instrument was obtained from Sun Chrome (SunCollect, Germany). Blast drying oven was obtained from Shanghai yiheng (Shanghai, China). AP MALDI ion source was purchased from Mass Tech (Columbia, USA).

TCMSP Database (https://www.tcmsp-e.com/tcmsp.php.); Herb Database (herb.ac.cn) Swiss database (http://www.swisstargetprediction.ch/); PubChem website (https://pubchem.ncbi.nlm.nih.gov/); PharmMapper Database: (PharmMapper (lilab-ecust.cn); GeneCards database (https://www.genecards.org/); Uniprot Database (www.uniprot.org); CTD Database (https://ctdbase.org); disgenet Database (Home (disgenet.cn)) String database (cn.string-db.org) David Database (david.ncifcrf.gov) HPA database (https://www.proteinatlas.org/); RCSB protein database (https://www.rcsb.org); Playmolecule database (https://open.playmolecule.org/landing); Venny software Cytoscape_v3.8.0 software AutoDock Vina software PyMol software.

2.4 Network pharmacological study of Fructus Chebulae for improvement of pharyngitis

2.4.1 Acquisition of effective active components and candidate targets of action in Fructus Chebulae

TCMSP and Herb databases were used to obtain the active ingredients of Fructus Chebulae. The search term is "hezi", and the duplicate content is removed after the search. The collected active ingredients were then screened according to the criteria of oral bioavailability (OB) ≥ 30% and drug similarity (DL) ≥0.18. The obtained active ingredients were screened in the Swiss Target Prediction database and PharmMapper databases to obtain the relevant targets of Fructus Chebulae, and the corresponding targets of the active ingredients obtained from TCMSP were merged and deduplicated, and then the target gene names were corrected according to the GeneCards database and Uniprot database. The species is defined as "Homosapiens", so as to obtain the corresponding target of the active ingredient of Fructus Chebulae.

2.4.2 Building a network of Fructus Chebulae - Pharyngitis - Active Ingredients - Targets of Action

Using the Genecards database (correlation score ≥ 1.0), the CTD database, and the DisGeNET database, potential targets for pharyngitis were searched with the keyword "pharyngitis", and the targets associated with pharyngitis were collected after merging and removing duplicate targets. It is beneficial for Venny software to draw a Venn diagram, showing the common target of Fructus Chebulae and "Pharyngitis", and identifying it as a potential target for Fructus Chebulae to treat pharyngitis, anti-inflammatory and swelling. Then, through the Cytoscape_v3.8.0 software, the active ingredient-target interaction network diagram was obtained.

2.4.3 Construction of protein-protein interaction networks

The obtained targets of Fructus Chebulae for the treatment of Pharyngitis were imported into the String database, and the species was limited to Homo sapiens, highest ≥ of 0.900, and the target protein-protein interaction networks (PPI) were constructed. Then, the Cytoscape_v3.8.0 software was used to visualize and analyze the PPI network. The MNC, MCC and EPC algorithms of cytoHubba were used for topological analysis, and the top 10 genes in the PPI network were determined.

2.4.4 Pathway and enrichment analysis

In order to further investigate the mechanism of Fructus Chebulae to improve pharyngitis, KEGG pathway analysis and GO enrichment analysis were performed on the obtained targets using the DAVID database (P value <0.01，FDR <0.01). The tissue distribution of the targets was then queried through THE HUMAN PROTEIN ATLAS database and the targets were classified according to heart, liver, spleen, lung, kidney and brain distribution. Finally, the active ingredients and targets of Fructus Chebulae, KEGG pathways related to inflammation and immunity, and the top 15 entries of each GO function were imported into Cytoscape software to construct the network of "Fructus Chebulae-pharyngitis-active ingredients-targets-pathways-main sites of action".

2.4.5 Analysis of molecular docking and forms of action of effective compounds

Molecular docking was performed using AutoDock software. The high-resolution crystal structures of the target proteins associated with the identified key active ingredients were downloaded from the RCSB protein database and required to be greater than the average degree in PPI analysis as the receptor protein for molecular docking, and the screening conditions were Organism(s): Homo sapiens, Method: X-ray diffraction, Resolution: best to worst, the release time is the latest. For the unknown crystal structure of the active pocket, upload the PDB file to the Playmolecule database for active pocket prediction. Then, according to the previous work such as the component-target interaction network, the highly biologically active components were determined to be ligand molecules, and their MOL2 format files were obtained. PyMol and AutoDock Vina software were used to remove ligands, dehydrate, hydrogenate, optimize charge, and finally, AutoDock Vina was used for molecular docking, and PyMol was used to visualize and analyze the docking results.

We further conducted in-depth molecular docking and molecular dynamics simulations between ellagic acid and SRC. The SRC protein crystal structure was retrieved from the RCSB Protein Data Bank. Water molecules, original ligands, and non-essential cofactors were removed using PyMol, followed by hydrogen addition. The

three-dimensional structure of ellagic acid was obtained from the TCMSP database, and its charges and atom types were assigned using AutoDockTools (ADT) before being saved in PDBQT format. Semi-flexible molecular docking was performed with AutoDock4.2. The binding pocket center was defined using ADT, and a grid box of 32 × 32 × 32 points with a spacing of 0.375 Å was set to cover the entire active site. Conformational searching was conducted using the Lamarckian genetic algorithm (LGA) with 200 runs, a population size of 150, and a maximum of 2.5 million evaluations. The docking results were ranked by binding free energy, and the lowest-energy conformation was selected for subsequent analyses. In parallel, the AlphaFold3 artificial intelligence model was employed to independently predict the ellagic acid-SRC complex structure for cross-validation of the docking reliability. Molecular dynamics simulations were carried out using GROMACS 2020.4 with the AMBER ff99SB force field. The complex was solvated in a TIP3P water box, and Na^+/Cl^- ions were added to neutralize the system and achieve a physiological salt concentration of 0.15 M. The system was energy-minimized to remove steric clashes, then equilibrated under NVT (100 ps) and NPT (100 ps) conditions to reach 300 K and 1 bar. A 200 ns production run was performed with a 2 fs time step, using Parrinello-Rahman pressure coupling and Langevin temperature coupling. The gmx rmsd tool was used to analyze backbone stability, gmx rmsf to evaluate residue flexibility, and the MM-PBSA method to calculate binding free energies and per-residue energy contributions.

2.5 Mechanism of action of Fructus Chebulae in improving pharyngitis

2.5.1 Modelling pharyngitis in mice

60 ♂ KM mice were randomly divided into two groups: the normal control group (10 animals) and the module group (50 animals). The pharyngeal spray stimulation was carried out with 5% ammonia (9:00 daily, 1 pinch per time, 50 μl per pamper), and the pharyngitis model was constructed by continuous intervention for 3 days. The normal control group received the same amount of normal saline spray at the same time. During the experiment, the activity status of mice was monitored daily, and the color, morphology and secretion characteristics of pharyngeal mucosa were evaluated by laryngoscope, and the body weight changes were recorded. After the pre-experiment confirmed the success of the modeling, 50 modeling mice were randomly divided into 5 groups (n=10): the model control group, the Lanqin oral solution treatment group (27.5 mg/kg), and the high (50 mg/kg), medium (30 mg/kg) and low (10 mg/kg) dose groups of ellagic acid. Spray administration (3 pinches of 50 μl per pinch was administered once a day at 9:00 and 17:00 p.m. daily) for 5 consecutive days. The normal control group and the model control group were treated with the same volume of 5% DMSO solution as the control, and the operation specifications of each group were consistent. After the last dose, the mice were fasted and watered, and 12 hours later, the eyeballs were removed

and sacrificed to death.

2.5.2 Data collection of body weight and organ mass

The change in body weight of the animals in each group was recorded daily from the first day during the experiment. The mass of each organ heart, liver, spleen, lungs and kidneys was recorded after sampling.

2.5.3 Endoscopic dynamic observation of pharyngeal appearances

The condition of the mice throat was observed daily during the experiment using a high-definition endoscope, and video and GIF motion pictures of the mice throat before sampling were taken after the last administration of the drug were filmed and recorded.

2.5.4 Histological examination

The pharyngeal and lung tissues of mice were fixed with 4% paraformaldehyde, paraffin-embedded, sectioned, HE stained, and the pathological changes of pharyngeal tissues were observed by light microscopy.

2.5.5 Detection of oxidative stress levels in pharyngeal and lung tissues

Pharyngeal and lung tissue samples were accurately weighed, 10% tissue homogenate was prepared in proportion, centrifuged at 4°C at 3000 rpm for 10 min, and the supernatant was taken to obtain a 10% concentration of pharyngeal and lung tissue homogenate stock solution. The above stock solution was taken and the protein content of pharyngeal and lung tissue samples was measured. The 10% tissue homogenate stock solution was sequentially diluted to determine the optimal detection concentration through pre-experiments, and the pharyngeal SOD and MDA samples were diluted 25-fold, and the lung samples were diluted 50-fold. Then, the SOD activity and MDA content of the pharyngeal and lung tissues of mice were detected according to the method of the kit.

2.5.6 Analysis of biochemical indicators in serum

After the last administration, the mice were fasted without food and water, and were killed by removing the eyeballs for blood 12 h later. The blood was extracted from the eyeballs and left at room temperature for 0.5-1 h. The serum was analyzed and centrifuged at 4 ℃ and 3 500 r/min for 15 min, and the TNF-α content in the serum was measured according to the method of the kit.

2.5.7 Immunoprotein fluorescence analysis

The pharyngeal and lung tissues of mice were fixed with 4% paraformaldehyde, paraffin-embedded, sectioned,

deparaffinized, antigen retrieval, goat serum blocking, primary antibody incubation, secondary antibody labeling, DAPI staining and post-nucleation mounting, and image information acquisition was performed using fluorescence microscopy to observe the difference in SRC target protein expression between pharyngeal and lung tissues.

2.6 Spatial metabolomics analysis

2.6.1 Preparation of sections

After the last administration, the mice were faxed and deprived of water. 12 hours later, the pharyngeal positions of the mice were quickly removed from the operating table and stored at -80℃. Then, the pharyngeal tissues of mice in the model group and the high-dose ellagic acid group were respectively placed in folded tin foil box-shaped molds (3 × 3 × 3cm), and 10% gelatin aqueous solution (gelatin: water = 1:10) was dropped into the molds as an embedding agent until the samples were completely covered. Subsequently, store it immediately in a refrigerator at -80℃ for 4 hours until the gelatin aqueous solution is completely opaque. Start the Thermo CRYOSTAR NX50 cryoslicer, pre-cool the freezer to -20℃, take out the pharyngeal tissues of the model group and the high-dose ellagic acid group mice from the -80℃ refrigerator, and place them in the freezer for equilibrium for 3 hours. Then, the sample was fixed on the sample head with the embedding liquid, the Angle and orientation were adjusted, and the sections were made according to the user manual of the slicer. The thickness of each section was 10 μm. Then, with the help of a pre-cooled brush, the sections were transferred onto the pre-cooled ITO conductive slides and dried for 20 minutes.

Start the circulating spray substrate spraying device (SunCollect, SunChrom), and spray the prepared sample sections with α-cyano-4-hydroxycinnamic acid CHCA (10 mg/ml 90% methanol + 0.1% trifluoroacetic acid) substrate. Spray 16 layers, and the nozzle temperature is at room temperature. The spraying speed is 1000 mm/min, and the flow rate of each layer of spraying varies in a gradient (10-60 μl/min).

2.7 Mass spectrometry imaging conditions

The Thermo Q Exactive Plus mass spectrometry detector (Thermo Fisher Scientific, USA) is connected in series with the AP/MALDI (ng) UHR ion source (MassTech, Columbia, MD), and the laser energy is set at 18%. Perform a first-level full scan in the positive ion ionization mode. The first-order ions are scanned within the range of 120-1000 m/z at a resolution of 35,000. The maximum ion implantation time (MIT) is set to 100 ms, the automatic gain control (AGCT) is 1e6, the isolation window m/z is set to 2, the capillary temperature is 320℃, and the S-lens RF level is 50%.

2.8 Statistics and analysis

In the MSI experiment, the AP-MALDI ion source scans the sample on the slide line by line, and then saves the mass spectrometry data obtained for each line as a RAW file. The reconstruction and visualization of mass spectrometry spatial images are realized based on the MSI processing algorithm. The MSI data were processed automatically using the biodeep software system platform (http://www.biodeep.cn). First, convert the RAW raw data file to the common mzML file format. Then, peak detection and peak quantification are carried out. The TrIQ algorithm is used to analyze and identify background noise and signal correction based on the detection intensity of the mass spectrometry ion signal. Dimensionality reduction is performed on the data respectively to subtract the background signal, and then downstream data analysis is conducted. Based on the unsupervised algorithm, the UMAP Manifold method was adopted to conduct dimension reduction and clustering analysis on the high-dimensional mass spectrometry imaging spatial data. Then, combined with the phenograph clustering algorithm, different typing regions and features on the slices were obtained. The regions with similar metabolite expression patterns and features were labeled with the same color. Then, combined with the spatial data filling algorithm, the division results with a high degree of consistency with the actual organizational distribution characteristics are obtained. Finally, based on the motif sequence search principle of the Gibbs sampling algorithm, the "conservativeness" of different single-ion layers in different regions was calculated and investigated. Among them, the closer the LDA value is to 1.00, the more "conservativeness" the ion is in the current region and can be regarded as a characteristic ion.

2.9 Multivariate statistical analysis

Firstly, it was beneficial to use the R software Ropls to conduct PLS-DA dimension reduction analysis on the sample data. The overfitting of the model was evaluated by using the permutation test method. R^2X and R^2Y are respectively used to quantify the degree of interpretation of the constructed model for the X matrix and the Y matrix, while Q^2 is used to characterize the predictive efficiency of the model. The closer the above indicators approach 1, the higher the goodness of fit of the model is, and the more accurately the samples in the training set can be classified into their original categories. To evaluate the influence degree and explanatory power of the content of each metabolite on the classification and discrimination of samples, and to assist in the screening of biomarker metabolites, the *P* value, VIP value and fold change were calculated to calculate the multiple of differences between groups. When the *P* value is less than 0.05 and the VIP value is greater than 1, it is determined that there are statistically significant differences in the corresponding metabolite molecules. For the differentially metabolized molecules screened out, this study used MetaboAnalyst to conduct functional pathway enrichment analysis and topological analysis. For the

enriched metabolic pathways, with the aid of the KEGG Mapper visualization tool, the visualization presentation and exploration of differential metabolites and pathway maps are achieved. The compound targets and disease targets of traditional Chinese medicine were obtained through the databases related to traditional Chinese medicine and disease targets. Network graph analyses such as GO enrichment analysis, KEGG enrichment analysis, PPI network analysis, compound - target - disease network, and compound - target - enrichment pathway was conducted on the common targets to further screen out the active ingredients and potential core targets.

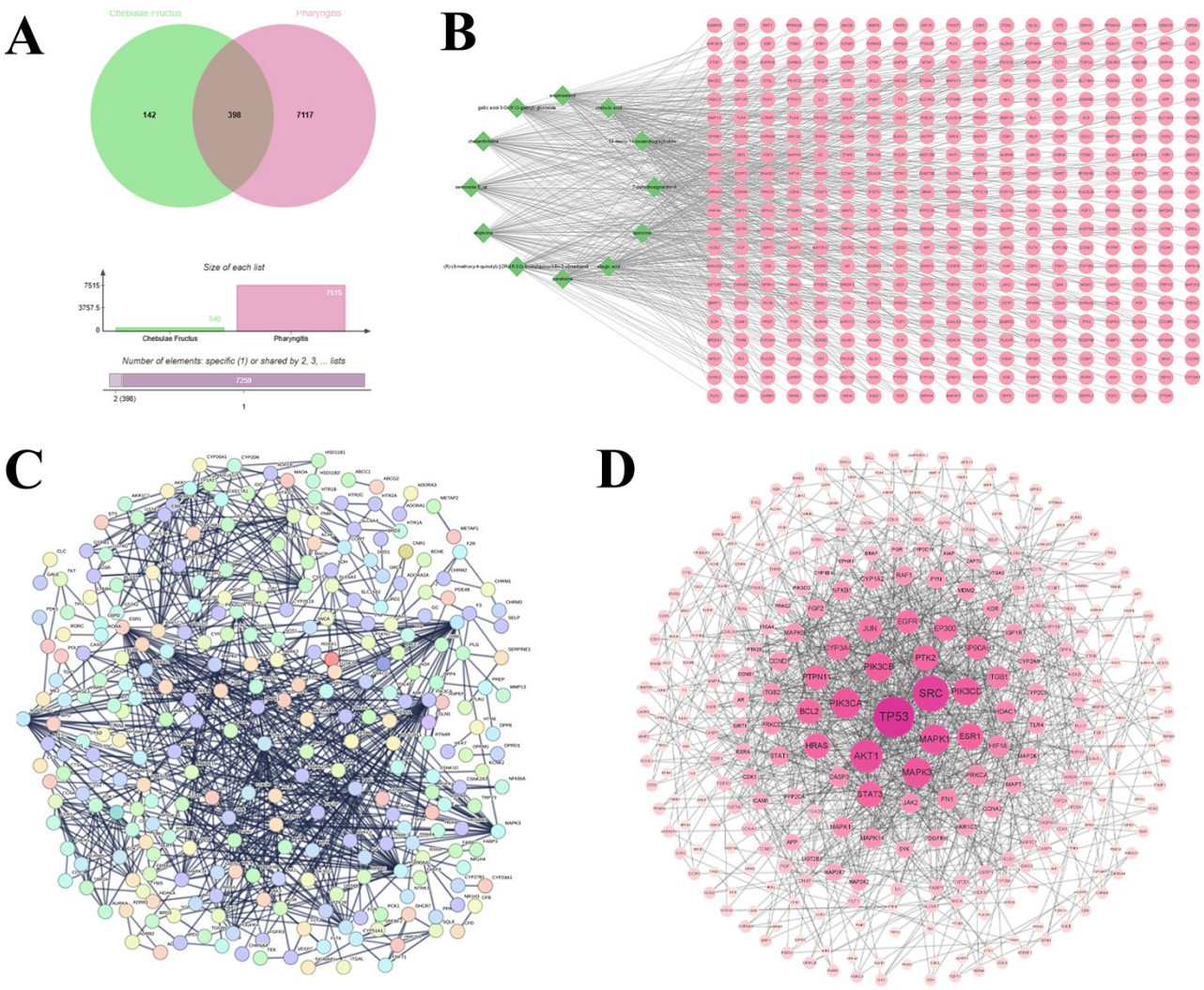

Figure S1. Venny plots of Fructus Chebulae active ingredient targets versus acute pharyngitis targets (A); Fructus Chebulae active ingredient-target-of-action gene network plots (B); PPI network plots of Fructus Chebulae active ingredient and acute pharyngitis intersecting targets (C); visualization of Fructus Chebulae active ingredient and acute pharyngitis core intersecting targets (D).

Table S1. Information on the 12 active ingredients of Fructus Chebulae.

Mol ID	Molecule Name	MW	OB （%）	DL
MOL001002	Ellagic acid	302.2	43.06	0.43
MOL002276	Sennoside E	524.5	50.69	0.61
MOL006376	7-Dehydrosigmasterol	414.79	37.42	0.75
MOL006826	Chebulic acid	356.26	72	0.32
MOL009135	Ellipticine	246.33	30.82	0.28
MOL009136	Peraksine	310.43	82.58	0.78
MOL009137	(R)-(6-methoxy-4-quinolyl)-[(2R,4R,5S)-5-vinylquinuclidin-2-yl] methanol	324.46	55.88	0.4
MOL009149	Cheilanthifoline	325.39	46.51	0.72
MOL008203	14-deoxy-11-oxoandrographolide	348.48	57.06	0.34
MOL004718	*α*-spinasterol	412.77	42.98	0.76
MOL000554	Gallic acid-3-*O*-(6'-*O*-galloyl)-glucoside	484.4	30.25	0.67
MOL011072	Quinicine	324.46	75.44	0.33

Table S2. Binding energy of ellagic acid from Fructus Chebulae to key targets (kcal/mol).

Name	SRC	ATK1	PTK2	NFKB1	FYN	BRAT	CDK4	IKBKB
PDB ID	8JN8	8R5K	6YOJ	9BOR	7A2P	8JNB	7OXW	4KIK
Affinity（kcal/mol）	-9.5	-6.8	-7.2	0	-6.9	-6.4	-5.9	-3.5

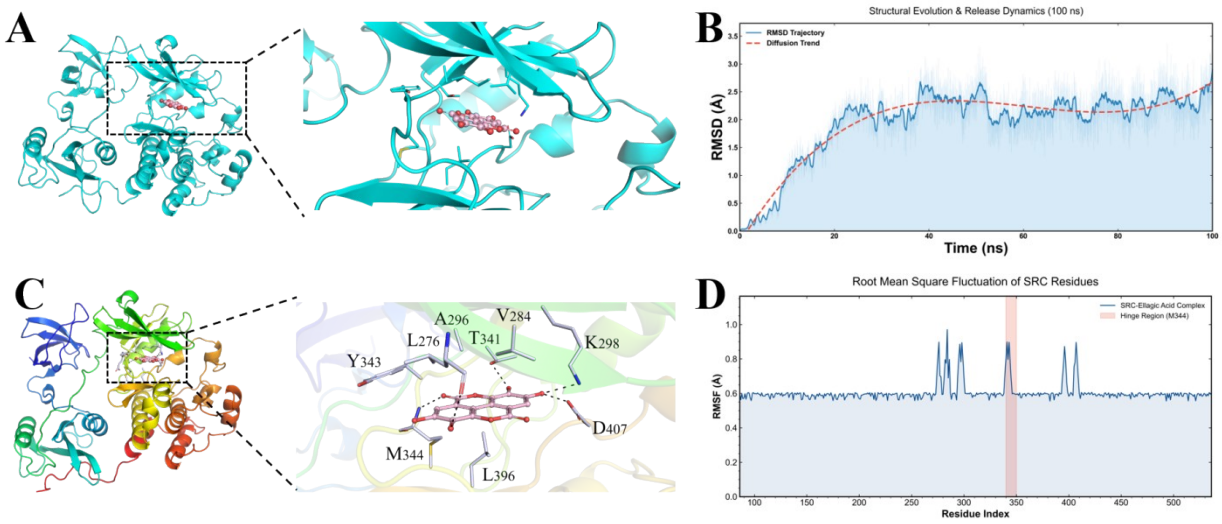

Figure S2. (A) AlphaFold3-predicted structure of the SRC-ellagic acid complex and close-up view of the binding site. (B) RMSD time curve of the SRC-ellagic acid system from molecular dynamics simulation. (C) Binding mode and interaction sites of the SRC-ellagic acid complex. (D) RMSF plot of SRC protein during the simulation.

Table S3. ROI regional analyses as well as statistics on the number of differential metabolites analyzed in the overall samples.

Comparison	Up	Down	Total_DE
H_A vs M_A	179	102	281
H_A vs M_B	87	92	179
H_A vs M_C	87	139	226
H_B vs M_A	110	107	227
H_B vs M_B	37	162	199
H_B vs M_C	50	158	208
H_C vs M_A	56	138	194
H_C vs M_B	76	156	232
H_C vs M_C	17	212	229
H vs M	154	222	376

Table S4. Detailed information on 49 pharmacodynamic biomarkers of ellagic acid for the treatment of acute pharyngitis in mice.

Name	Formula	Exact_mass	*m/z* (theoretic)	ppm	Precursor	MS level
2-Hydroxycinnamic acid	$C_9H_8O_3$	164.0473	147.0434	4.442	$[M+H-H_2O]^+$	2
3-Dehydroquinic acid	$C_7H_{10}O_6$	190.0477	191.0522	14.721	$[M+H]^+$	2
Calcidiol	$C_{27}H_{44}O_2$	400.3341	401.3399	3.710	$[M+H]^+$	2
Cholesterin	$C_{27}H_{46}O$	386.3548	369.3502	3.677	$[M+H-H_2O]^+$	1
D-Mannitol	$C_6H_{14}O_6$	182.0790	200.1135	3.199	$[M+NH_4]^+$	1
Kynurenic acid	$C_{10}H_7NO_3$	189.0426	172.0384	5.247	$[M+H-H_2O]^+$	2
L-Arginine	$C_6H_{14}N_4O_2$	174.1117	213.2065	13.704	$[M+K]^+$	2
D-Ribulose 5-phosphate	$C_5H_{11}O_8P$	230.0192	230.0415	3.973	$[M-H_2O+NH_4]^+$	1
Dodecenedioate （C12:1-DC）	$C_{12}H_{20}O_4$	228.1362	229.1404	13.216	$[M+H]^+$	1
Dopamine	$C_8H_{11}NO_2$	153.0790	136.0752	3.572	$[M+H-H_2O]^+$	2
5-Amino-6-(5'-phosphoribitylamino) uracil	$C_9H_{17}N_4O_9P$	356.0733	357.0832	7.313	$[M+H]^+$	1
Aconitate [cis or trans]	$C_6H_6O_6$	174.0164	174.0380	9.757	$[M-H_2O+NH_4]^+$	1
Adenine	$C_5H_5N_5$	135.0545	136.0613	3.450	$[M+H]^+$	1

Anserine	$C_{10}H_{16}N_4O_3$	240.1222	240.1446	3.727	$[M-H_2O+NH_4]^+$	1
Carnosine	$C_9H_{14}N_4O_3$	226.1066	226.1289	4.183	$[M-H_2O+NH_4]^+$	1
Creatine	$C_4H_9N_3O_2$	131.0695	132.0763	3.406	$[M+H]^+$	2
Cytidine	$C_9H_{13}N_3O_5$	243.0855	261.1220	10.178	$[M+NH_4]^+$	1
L-Cystathionine	$C_7H_{14}N_2O_4S$	222.0674	240.0990	9.370	$[M+NH_4]^+$	1
L-Homocystine	$C_8H_{16}N_2O_4S_2$	268.0551	286.0886	1.297	$[M+NH_4]^+$	1
L-Lysine	$C_6H_{14}N_2O_2$	146.1055	129.1019	2.586	$[M+H-H_2O]^+$	2
L-Phenylalanine	$C_9H_{11}NO_2$	165.0790	148.0751	3.958	$[M+H-H_2O]^+$	2
L-Tyrosine	$C_9H_{11}NO_3$	181.0739	164.0699	4.273	$[M+H-H_2O]^+$	2
Maltotriose	$C_{18}H_{32}O_{16}$	504.1690	504.1730	8.968	$[M]^+$	1
Mannose 6-phosphate	$C_6H_{13}O_9P$	260.0297	283.0173	5.789	$[M+Na]^+$	1
N-acetyl-aspartyl-glutamate (NAAG)	$C_{11}H_{16}N_2O_8$	304.0907	304.0912	3.575	$[M]^+$	1
Niacinamide	$C_6H_6N_2O$	122.0480	140.0813	3.826	$[M+NH_4]^+$	2
Pyridoxine 5'-phosphate	$C_8H_{12}NO_6P$	249.0402	250.0464	4.394	$[M+H]^+$	2
Spermidine	$C_7H_{19}N_3$	145.1579	146.1646	3.871	$[M+H]^+$	2
Spermine	$C_{10}H_{26}N_4$	202.2157	203.2223	3.504	$[M+H]^+$	1
beta-Alanyl-L-arginine	$C_9H_{19}N_5O_3$	245.1488	228.1447	3.479	$[M+H-H_2O]^+$	2
Phosphonoacetaldehyde	$C_2H_5O_4P$	123.9925	146.9811	4.536	$[M+Na]^+$	2

Selenodiglutathione	$C_{20}H_{32}N_6O_{12}S_2Se$	692.0685	657.0632	13.054	$[M+H-2H_2O]^+$	1
5-Hydroxy-L-tryptophan	$C_{11}H_{12}N_2O_3$	220.0848	221.0910	4.815	$[M+H]^+$	2
5-Hydroxyindoleacetylglycine	$C_{12}H_{12}N_2O_4$	248.0797	248.0996	13.558	$[M-H_2O+NH_4]^+$	1
5-Methoxytryptamine	$C_{11}H_{14}N_2O$	190.1106	208.1436	4.001	$[M+NH_4]^+$	1
Biotin	$C_{10}H_{16}N_2O_3S$	244.0882	283.1870	3.849	$[M+K]^+$	2
Dehydroepiandrosterone sulfate	$C_{19}H_{28}O_5S$	368.1657	333.1517	0.547	$[M+H-2H_2O]^+$	1
Estrone glucuronide	$C_{24}H_{30}O_8$	446.1941	447.1963	11.258	$[M+H]^+$	1
Hordenine	$C_{10}H_{15}NO$	165.1154	148.1115	3.845	$[M+H-H_2O]^+$	1
Kynurenine	$C_{10}H_{12}N_2O_3$	208.0848	226.1177	4.040	$[M+NH_4]^+$	2
L-Formylkynurenine	$C_{11}H_{12}N_2O_4$	236.0797	236.0997	13.823	$[M-H_2O+NH_4]^+$	1
L-Tryptophan	$C_{11}H_{12}N_2O_2$	204.0899	222.1219	8.097	$[M+NH_4]^+$	2
Methylimidazole acetaldehyde	$C_6H_8N_2O$	124.0637	125.0706	2.688	$[M+H]^+$	1
N-alpha-acetylornithine	$C_7H_{14}N_2O_3$	174.1004	157.0966	3.494	$[M+H-H_2O]^+$	2
Nicotinic acid ribonucleoside	$C_{11}H_{14}NO_6^+$	256.0821	257.0905	4.338	$[M+H]^+$	1
Riboflavin (Vitamin B2)	$C_{17}H_{20}N_4O_6$	376.1383	394.1741	5.065	$[M+NH_4]^+$	2
Serotonin	$C_{10}H_{12}N_2O$	176.0950	159.0911	3.580	$[M+H-H_2O]^+$	2
Xanthine	$C_5H_4N_4O_2$	152.0334	152.0561	3.846	$[M-H_2O+NH_4]^+$	2

Glucosamine	$C_6H_{13}NO_5$	179.0794	179.0785	1.788	$[M]^+$	1